4.2 RECENT PROGRESS IN THE DEVELOPMENT OF DUCTILE-PHASE TOUGHENED TUNGSTEN FOR PLASMA-FACING MATERIALS: W-Ni-Fe COMPOSITES – C. H. Henager, Jr., E. L. Stevens, R. J. Kurtz, T. J. Roosendaal, E. A. Nyberg, C. A. Lavender (Pacific Northwest National Laboratory), G. R. Odette, K. H. Cunningham, and F. W. Zok (University of California, Santa Barbara)

OBJECTIVE

The objective of this study is to fabricate, test, and characterize a lamellar W-Ni-Fe composite based on tungsten heavy metal alloys suitable for model material development for fusion reactor studies of ductile-phase toughening. The lamellar structure will be obtained by hot-rolling the as-sintered W-Ni-Fe composite.

SUMMARY

A promising approach to increasing fracture toughness and decreasing the DBTT of a W-alloy is by ductile-phase toughening (DPT) [1-3]. In this method, a ductile phase is included in a brittle matrix to prevent fracture propagation by crack bridging or crack deflection. Liquid-phase sintered W-Ni-Fe alloys consisting of nearly spherical W-particles embedded within a Ni-Fe-W ductile matrix are being manipulated by hot-rolling to create lamellar W/Fe-Ni-W composites with anisotropic fracture properties. The rolled W-Ni-Fe alloy becomes a lamellar alloy consisting of W lamellae separated by ductile-phase regions. The W-rich lamellae are strong but brittle, while the ductile-phase metallic regions have a thin, plate-like morphology to provide a ductile bridging region. This rolled material is oriented with the W-rich lamellae parallel to principal stresses so that surface cracking is normal to the ductile-phase bridging regions.

PROGRESS AND STATUS

Background

Tungsten (W) and W-alloys are the solid materials of choice for plasma-facing components (PFCs) of future fusion reactors, such as the International Thermonuclear Experimental Reactor (ITER) and Demonstration Power Plant (DEMO), due to their high melting point, strength at high temperatures, high thermal conductivity, low coefficient of thermal expansion, and low sputtering yield [4-8]. However, W and most W-alloys exhibit low fracture toughness and a high ductile-brittle transition temperature (DBTT) that would render them as brittle materials during reactor operations [4, 6, 9]. The DBTT for unirradiated W-alloys typically ranges from 573K to 1273K (300 to 1000˚C) and in a reactor environment radiation hardening would further elevate this range [6, 10, 11]. W-alloys toughened by engineered reinforcement architectures, such as ductile-phase toughening (DPT), are strong candidates for PFCs. In DPT, a ductile phase is included in a brittle matrix to prevent fracture propagation. The principles of DPT are illustrated in Figure 1, which shows an actual and schematic illustration of ductile bridging ligaments stretching across an open crack in a brittle matrix material, such as W [12, 13].

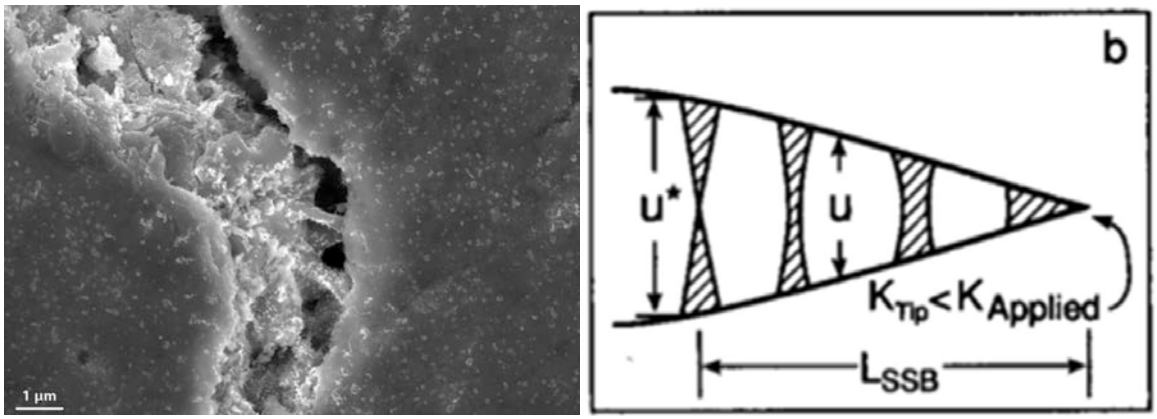

Figure 1. (a) SEM image of W-Cu fracture where the ductile phase (Cu) is effectively bridging the crack. (b) A steady-state bridging zone shown schematically in 2D [13].

Experimental

W-Ni-Fe alloys, purchased as green bodies consisting of W-7%Ni-3%Fe[1], were prepared for testing using hot-rolling to provide a range of lamellar microstructures with anisotropic fracture behavior. The starting alloy shown in Figure 2 is formed using liquid phase sintering methods and exhibits an isotropic structure consisting of W-spheroidal particles embedded in a Fe-Ni-W matrix. The W-particles are very close to 100% W. The matrix, basically a Ni-based superalloy, is 52.2-56.9% Ni, 25.8-29.3% W, and 13.8-21.6% Fe by wt%.

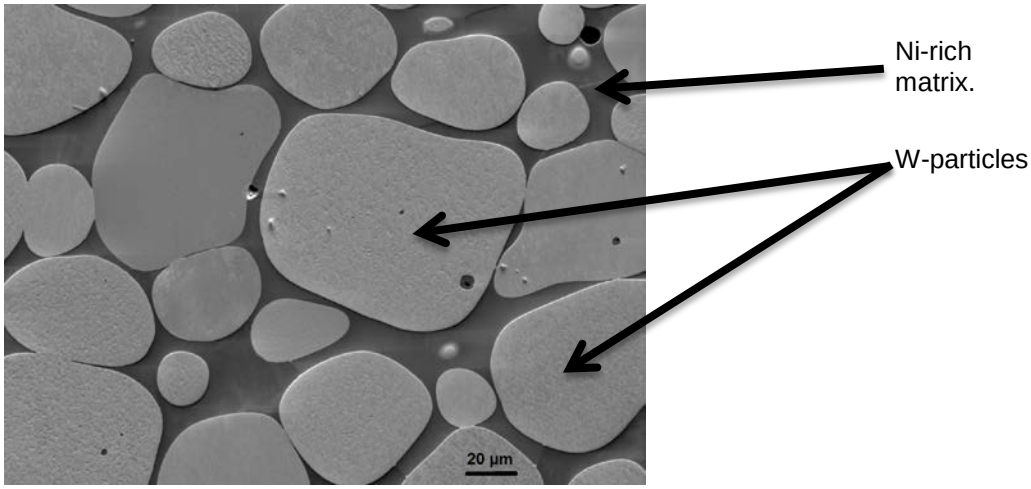

Figure 2. W-Ni-Fe alloy showing W-particles and Ni-rich ductile matrix.

These alloys were hot-rolled to three different reduction percentages, in two series of hot-roll/annealing sequences. The first rolling sequence was performed at 1150˚C for two passes with 5% reduction per rolling pass after the initial sintering. Then the alloys are rolled at 900˚C in 11% reduction passes to 62% reduction and 74% reduction. After three passes the materials are annealed at 900˚C for 1 hour in Ar-H (50:50) atmosphere. The second rolling sequence was similar but was started using a thicker plate and rolled to 87% reduction. Following this reduction samples were then hydrogen de-gassed at 900˚C in

[1] Mi-Tech Metals, Indianapolis, IN, USA.

vacuum. Figure 3 shows SEM images of the as-rolled materials at different reduction percentages. Note that only the 87% reduced material resembles a lamellar structure with highly elongated W-particles.

Four-point single-edge notched bend (SENB) specimens measuring 25.4 mm x 1.75 mm x 4.0 mm were cut from pieces with total reductions of 62%, 74%, and 87% (labeled R62, R74, and R87, respectively). The notch depth, a, was set at 0.45 a/W, where W was 4.0 mm. Three samples from each reduction amount were tested at room temperature using 0.2 mm/min displacement rate until failure in an Instron 5500 test frame equipped with a 4-point bend mid-point displacement transducer. Representative load-displacement curves for each are shown in Figure 4**.** Note that the hydrogen de-gassing treatment increased the fracture resistance of the 87% reduction material but decreased that for the 62% and 74%. The reasons for this difference in response are not yet understood, but it was expected that hydrogen de-gassing would improve the overall fracture resistance by increasing the toughness of the Ni-rich matrix phase. That appeared to be the case for the 87% reduction material.

Each tested sample was then polished and examined with optical and scanning electron microscopy. Crack morphology and propagation path were evaluated by visual inspection of the micrographs, shown in Figures 5 and 6. It was observed that there were significant differences between the 62% and 74% crack morphologies compared to the 87% reduced materials in the form of additional crack deflection and crack tortuosity. Figure 6 reveals that near the crack-tip differences are more pronounced but that all the rolled samples exhibit crack bridging toughening with fracture through the W-particles.

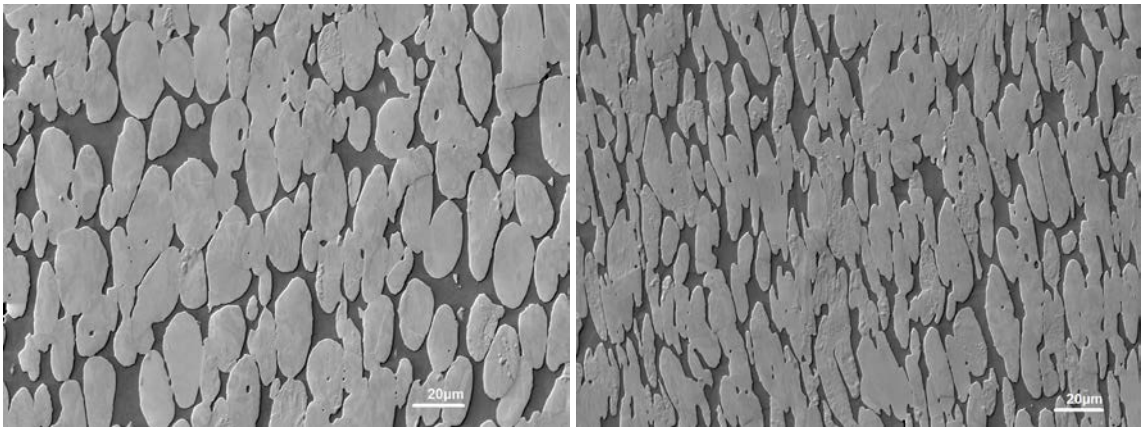

(a) 62% (b) 74%

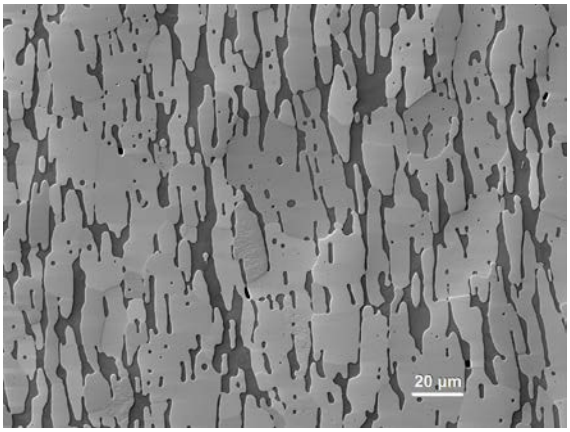

(c) 87%

Figure 3. SEM images of hot-rolled W-Ni-Fe alloy with (a) 62%, (b) 74%, and (c) 87% reductions, respectively. These rolled materials were tested with the specimens oriented so that crack growth was horizontal (right to left) in the image.

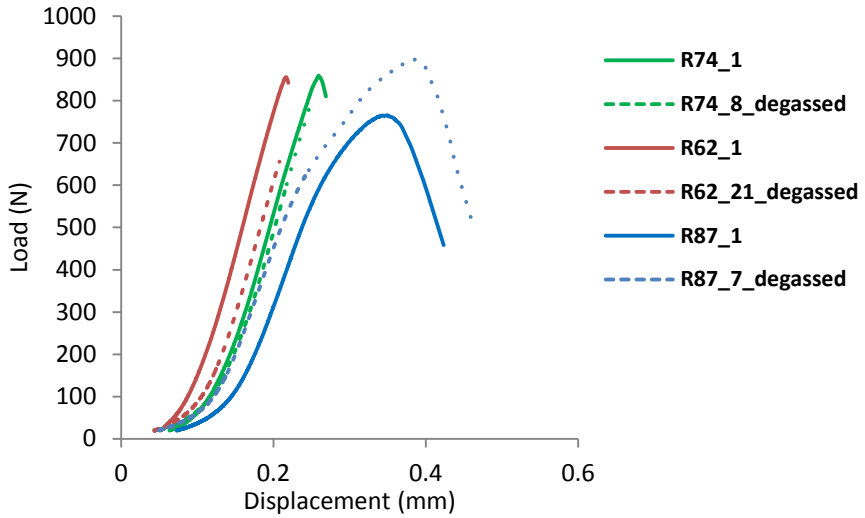

Figure 4. Representative load-displacement curves for R62, R74, and R87 4-point SENB specimens before and after hydrogen de-gassing.

Interaction of the growing crack with W-particle crystallography was assessed using electron backscatter diffraction (EBSD) as shown in Figure 7. Some particles fractured along grain boundaries, while others fractured through grains via transgranular cleavage. The EBSD data showed that the majority of the W-particles are single grains but that some appear to be polycrystalline. The images suggest that polycrystalline W-particles are formed by agglomeration of single crystal particles during the rolling operation. An EDS phase mapped image shows that cracks deflect between the W-particles (red) and the Ni-rich matrix phase (blue) and that many of the cracks stop within the Ni-rich phase. Figure 8 is a higher magnification image of a crack in a tested W-Ni-Fe sample that shows a flat cleavage face of a W-particle (A) and the more ductile-like fracture surface of the Ni-rich matrix phase (B). A series of crack-tip bridges along with crack debonding are shown in Figure 9 for the 87% reduction material. Crack bridging is accompanied by crack deflection due to significant debonding between the brittle W-particles and the ductile Ni-rich matrix phase. The formation of crack-tip debonding is critical to the formation of crack-tip bridges.

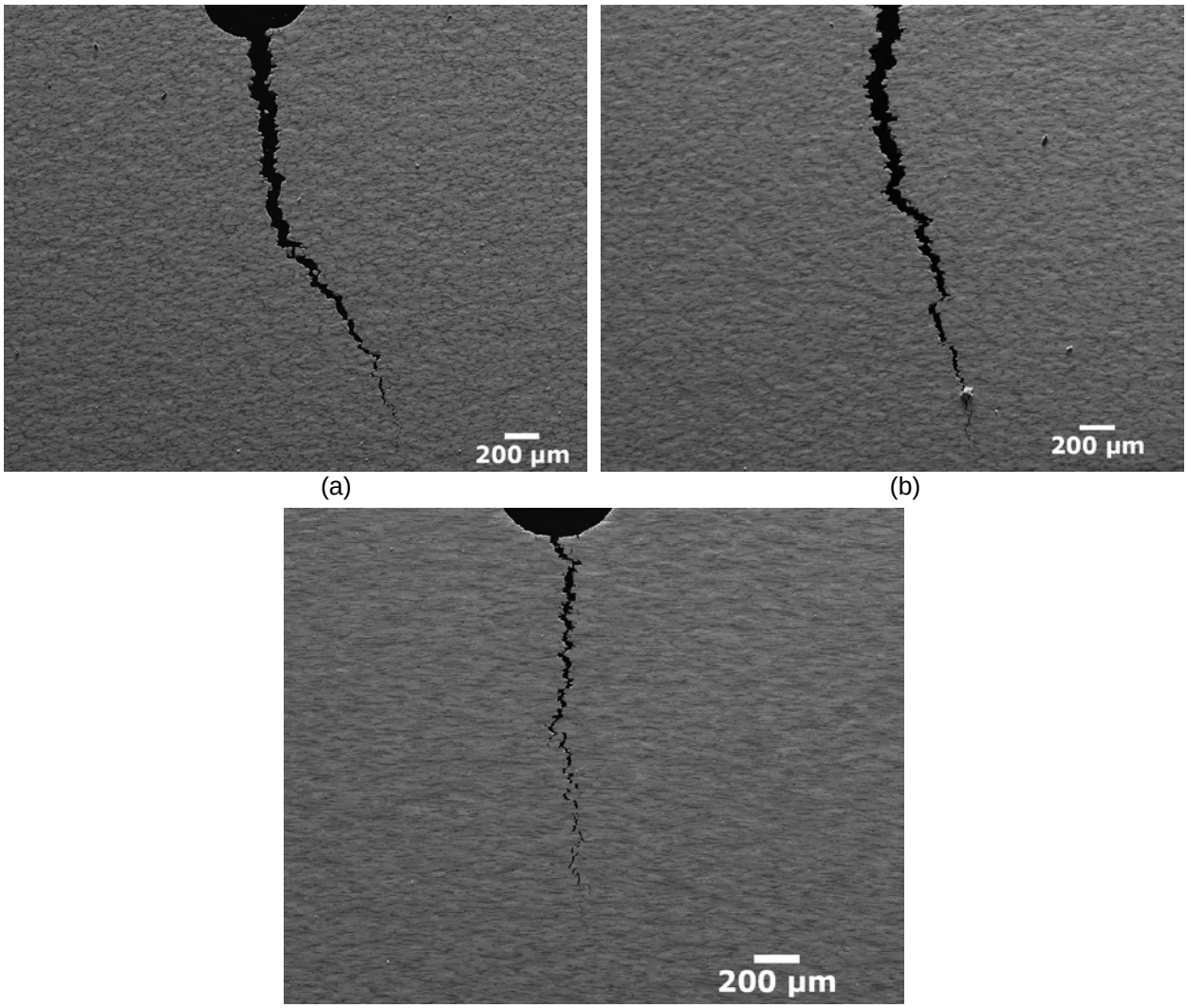

(a) (b)

(c)

Figure 5. Scanning electron (secondary image) micrographs of crack morphologies observed in SENB specimens tested in 4-point bending at 0.2 mm/min at ambient temperature. Shown in (a) is 62%, (b) 74%, and (c) 87% hot-rolled reduction prior to hydrogen degassing. These samples correspond to the load-displacement curves shown in Figure 3 above. Note the crack path deflection seen in the 87% rolled sample is more pronounced compared to 62% and 74% reductions. This is better seen in the higher magnification images shown in Figure 6 below.

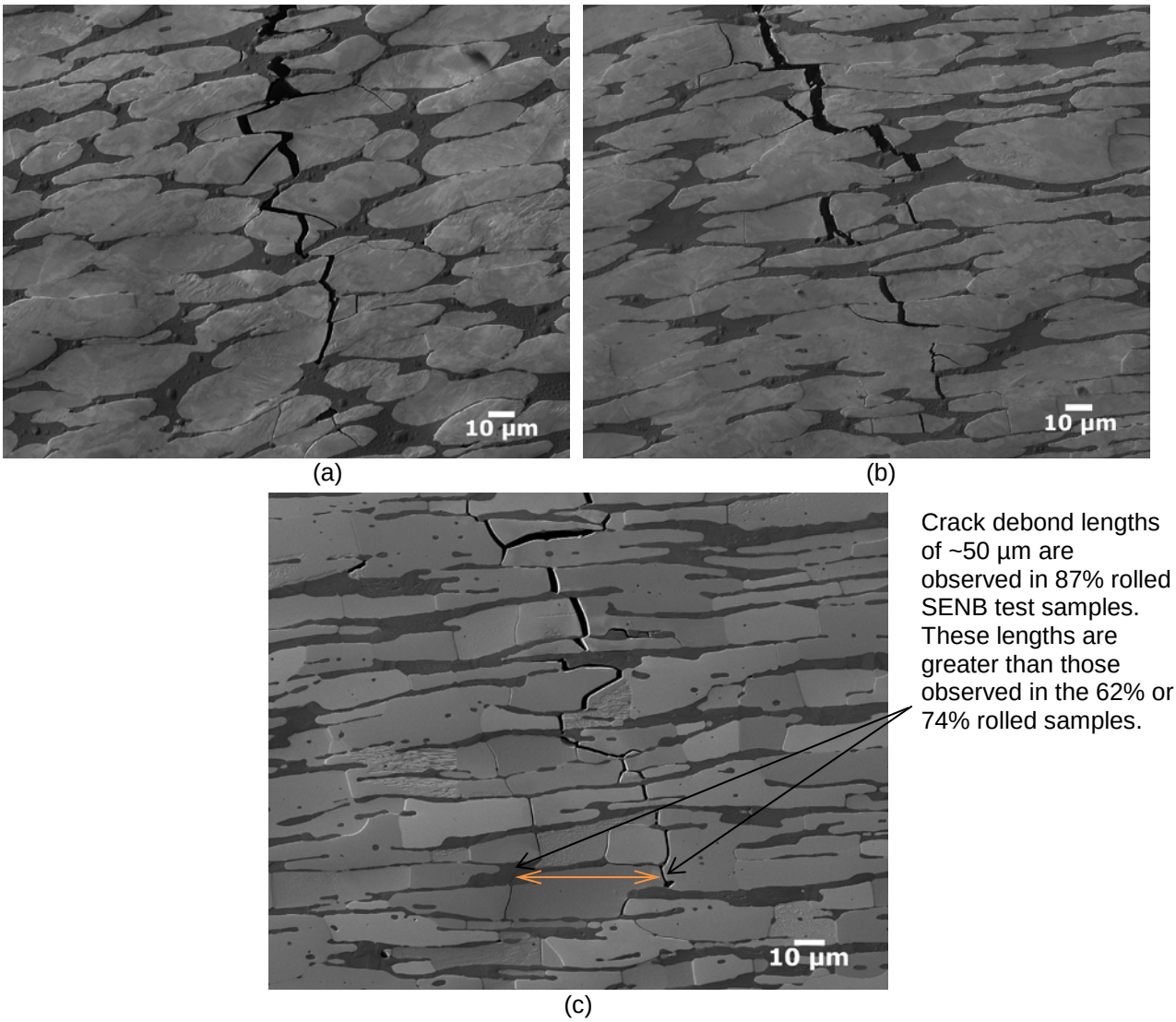

(a) (b) (c)

Figure 6. SEM micrographs of crack-tip morphologies taken at 500x showing crack deflection, crack bridging, and crack nucleation in all rolled samples as in (a) 62%, (b) 74%, and (c) 87%. Crack deflection is more pronounced in the 87% reduced sample but is observed in all rolled materials. Measured crack debond lengths (the length between parallel cracks) approaches 50 µm for the 87% rolled material.

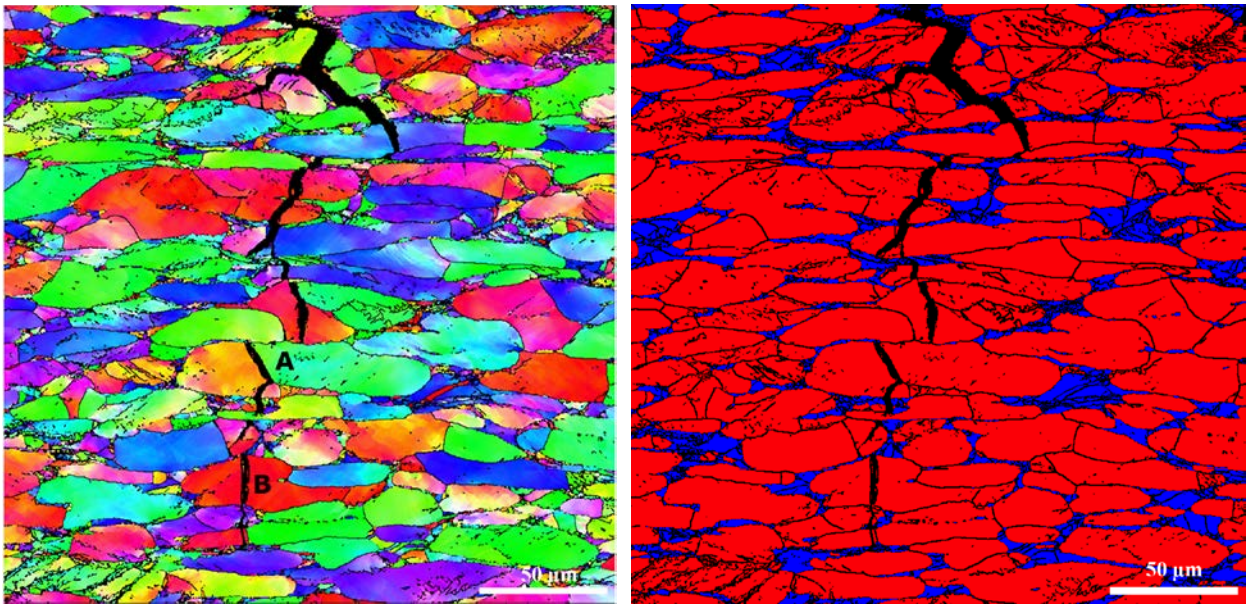

(a) (b)

Figure 7. (a) SEM EBSD inverse pole figure along the z-direction for a 62% reduction sample, showing intergranular cracking (A) and transgranular cleavage (B). This behavior was observed also in the 74% and 87% reduction samples. Shown in (b) is an EDS phase map of the image in (a) with W shown in red and the ductile Ni-rich matrix phase shown in blue. This figure highlights the crack bridging and deflection occurring at the phase boundaries in this rolled composite.

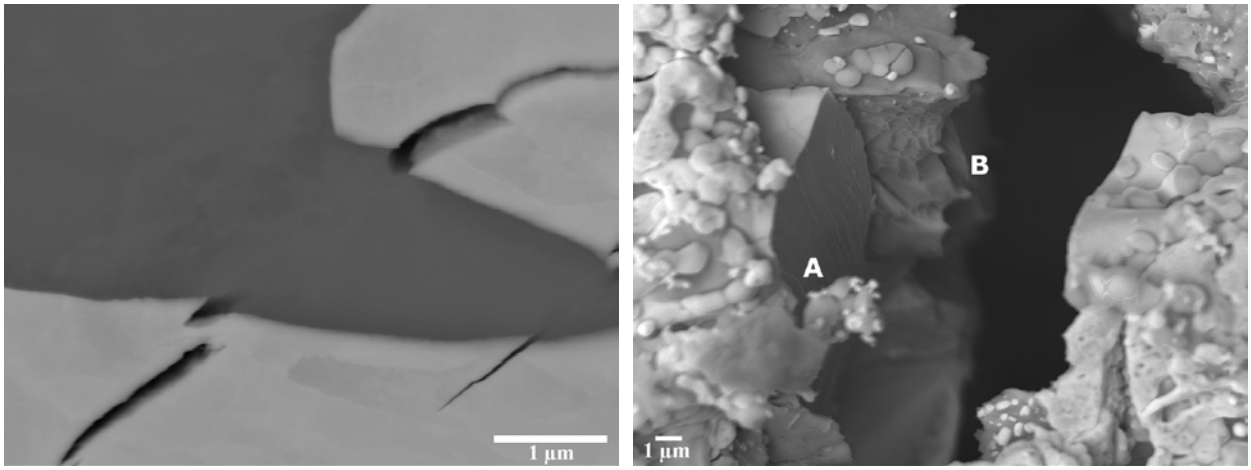

(a) (b)

Figure 8. (a) SEM backscatter image showing matrix phase (dark) bridging a crack in W-particles. Shown in (b) is an SEM image inside a crack in one of the tested composites showing transgranular cleavage fracture of W-particle in A and a more ductile tearing fracture of the Ni-rich phase in B.

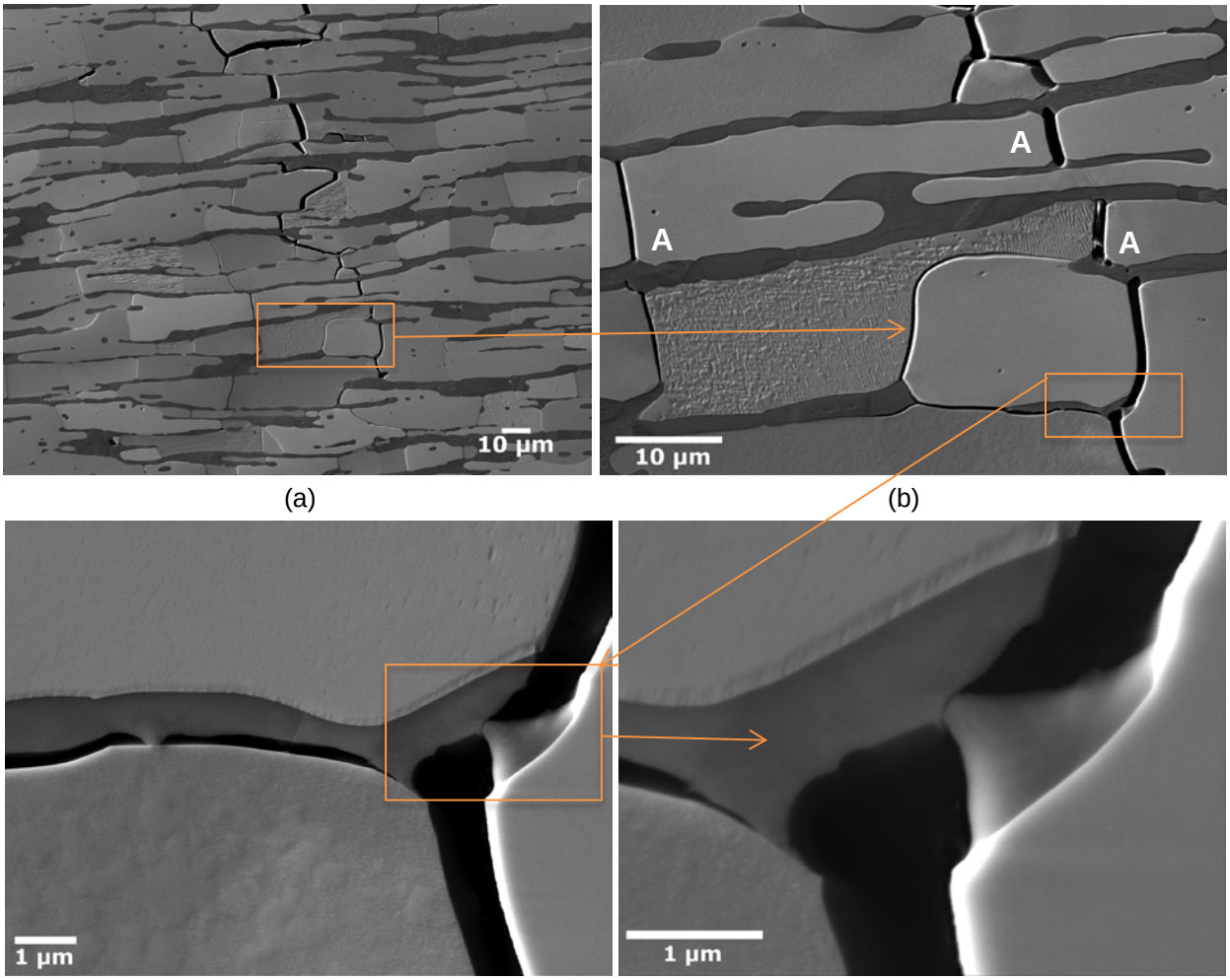

(a) (b) (c) (d)

Figure 9. A sequence of SEM images of increasing magnification for the 87% rolled and tested sample. Shown in (a) is a 500x image of the crack-tip region with the image in (b) showing the debonding associated with the crack deflection. The image shown in (c) highlights several Ni-rich bridges that are formed along the debond. The image in (d) is at 27kx and shows a partially intact bridge region. Areas marked with A in (b) illustrate cracks in the W-particles that are blunted in the Ni-rich matrix layers.

Discussion

In contrast to the W-Cu alloys that consist of Cu-particles embedded within a pure W-matrix, these W-Ni-Fe alloys consist of W-particles embedded within a Ni-Fe-W matrix phase. This material can be hot-rolled to produce nearly pure W-lamellae embedded within a lamellar Ni-rich ductile phase that behaves like a dual-phase composite, i.e. a ductile-phase composite. The as-sintered starting alloy fractures almost entirely within the Ni-rich matrix phase and, therefore, does not engage the W-phase as desired. The rolled alloys, in contrast, fracture by transgranular cleavage (mostly) in the highly elongated W-particles and ductile tearing of the Ni-rich phase that occupies the space between the pancake-shaped rolled W-particles. The cracking is accompanied by significant debonding, crack deflection, and crack bridging in all of the rolled alloys tested here. This initial work has shown that 87% reduction by hot rolling performs better than rolled reductions of 62% or 74% in terms of graceful failure as indicated by the load-displacement curves shown in Figure 4. Micrographs confirm the formation of a suitable lamellar structure at the rolling reduction amount of 87%. This lamellar structure behaved in a more ductile manner in 4-point SENB testing than the 62% and 74% reduction samples.

The observation of toughness improvement with increased rolling reduction appears to be a type of threshold that occurs when the W-particles reach a certain eccentricity. The 4-point SENB testing

suggests that a critical threshold occurs between 74% and 87% rolling reduction such that a significant increase in crack deflection begins to occur during crack propagation in the 87% rolled material (see Figure 5c). If this is the case, then increases in crack debonding lengths act to increase the volume of ductile-phase regions that interact with the crack and result in a more effective crack-bridging zone. This appears to be the case as shown in Figure 6c. This will have to be more completely verified and validated by further testing, additional characterization, and modeling.

The SEM EBSD and EDS phase mapping analysis in Figure 7 shows that W-particles fracture both through grains as transgranular cleavage cracks as well as intergranularly. However, most W-particles in the observed area consisted of single grains, which necessarily precluded grain boundary cracking. An image of a transgranular cleavage crack face is seen in Figure 8. It might be the case that W-particle interfaces are from two W-particles agglomerating during the hot-rolling operation. Research in these alloys by others indicates that transgranular cleavage is preferred over intergranular fracture or decohesion [14]. The presence of cleavage cracking indicates a high degree of bonding between the ductile matrix phase and the W-particles, whereas the intergranular strength of these alloys is thought to be rather low due to impurities. Maximum ductility, or toughness, of deformed W-Ni-Fe alloys is observed when there is a good combination of W-particle cleavage and ductile-phase rupture [14].

Future Work

Further testing and microscopy are planned to explore the crack deflection hypothesis discussed above. Additional testing, advanced characterization, and quantitative metallography are planned. A bridging model and an FE model are being explored for microstructural modeling of the SENB data. Exploration of alternative alloy compositions that reduce the amount of Ni in the alloy to alleviate neutron activation concerns will follow successful fracture testing and model validation.

References

[1] Deve, H.E., A.G. Evans, G.R. Odette, R. Mehrabian, M.L. Emiliani, and R.J. Hecht, "Ductile reinforcement toughening of -TiAl: effects of debonding and ductility," Acta metallurgica et materialia, (1990), 38(8), 1491-502.

[2] Erdogan, F. and P.F. Joseph, "Toughening of ceramics through crack bridging by ductile particles," Journal of the American Ceramic Society, (1989), 72(2), 262-270.

[3] Sigl, L.S., P.A. Mataga, B.J. Dalgleish, R.M. McMeeking, and A.G. Evans, "On the Toughness of Brittle Materials Reinforced with a Ductile Phase," Acta Metallurgica, (1988), 36(4), 945-953.

[4] Rieth, M., J.L. Boutard, S.L. Dudarev, T. Ahlgren, S. Antusch, N. Baluc, M.F. Barthe, C.S. Becquart, L. Ciupinski, J.B. Correia, C. Domain, J. Fikar, E. Fortuna, C.C. Fu, E. Gaganidze, T.L. Galan, C. Garcia-Rosales, B. Gludovatz, H. Greuner, K. Heinola, N. Holstein, N. Juslin, F. Koch, W. Krauss, K.J. Kurzydlowski, J. Linke, C. Linsmeier, N. Luzginova, H. Maier, M.S. Martinez, J.M. Missiaen, M. Muhammed, A. Munoz, M. Muzyk, K. Nordlund, D. Nguyen-Manh, P. Norajitra, J. Opschoor, G. Pintsuk, R. Pippan, G. Ritz, L. Romaner, D. Rupp, R. Schaublin, J. Schlosser, I. Uytdenhouwen, J.G. Van Der Laan, L. Veleva, L. Ventelon, S. Wahlberg, F. Willaime, S. Wurster, and M.A. Yar, "Review on the EFDA programme on tungsten materials technology and science," Journal of Nuclear Materials, (2011), 417, 463-467.

[5] Pitts, R.A., A. Kukushkin, A. Loarte, A. Martin, M. Merola, C.E. Kessel, V. Komarov, and M. Shimada, "Status and physics basis of the ITER divertor," Physica Scripta Volume T, (2009), 2009(T138), 014001 (10 pp.).

[6] Mertens, P., T. Hirai, M. Knaup, O. Neubauer, V. Philipps, J. Rapp, V. Riccardo, S. Sadakov, B. Schweer, A. Terra, I. Uytdenhouwen, and U. Samm, "A bulk tungsten divertor row for the outer strike point in JET," Fusion Engineering and Design, (2009), 84(7-11), 1289-93.

[7] Gervash, A., R. Giniyatulin, T. Ihli, W. Krauss, A. Makhankov, I. Mazul, P. Norajitra, and N. Yablokov, "Fabrication of a He-cooled divertor module for DEMO reactor," Journal of Nuclear Materials, (2007), 367-370 B(SPEC. ISS.), 1472-1475.

[8] Merola, M., W. Danner, and M. Pick, "EU RD on divertor components," Fusion Engineering and Design, (2005), 75-79(SUPPL.), 325-331.

[9] Mertens, P., V. Philipps, G. Pintsuk, V. Riccardo, U. Samm, V. Thompson, and I. Uytdenhouwen, "Clamping of solid tungsten components for the bulk W divertor row in JET-precautionary design for a brittle material," Physica Scripta Volume T, (2009), (T138), 014032 (5 pp.).
[10] Gludovatz, B., S. Wurster, A. Hoffmann, and R. Pippan, "Fracture toughness of polycrystalline tungsten alloys," International Journal of Refractory Metals and Hard Materials, (2010), 28(6), 674-8.
[11] Zinkle, S.J. and N.M. Ghoniem, "Operating temperature windows for fusion reactor structural materials," Fusion Engineering and Design, (2000), 51-52, 55-71.
[12] Venkateswara Rao, K.T., G.R. Odette, and R.O. Ritchie, "Ductile-reinforcement toughening in -TiAl intermetallic-matrix composites: effects on fracture toughness and fatigue-crack propagation resistance," Acta Metallurgica et Materialia, (1994), 42(3), 893-911.
[13] Odette, G.R., B.L. Chao, J.W. Sheckherd, and G.E. Lucas, "Ductile phase toughening mechanisms in a TiAl-TiNb laminate composite," Acta metallurgica et materialia, (1992), 40(9), 2381-9.
[14] Ostolaza Zamora, K.M., J.G. Sevillano, and M. Fuentes Pérez, "Fracture toughness of W heavy metal alloys," Materials Science and Engineering: A, (1992), 157(2), 151-160.